Nat. Hazards Earth Syst. Sci. Discuss., 1, 2353–2395, 2013
www.nat-hazards-earth-syst-sci-discuss.net/1/2353/2013/
doi:10.5194/nhessd-1-2353-2013

Natural Hazards and Earth System Sciences
Discussions

Temporary seismic monitoring of the Sulmona area (Abruzzo, Italy): quality study of microearthquake locations

M. A. Romano[1,2], R. de Nardis[1,3], M. Garbin[2], L. Peruzza[2], E. Priolo[2], G. Lavecchia[1], and M. Romanelli[2]

[1]GeosisLab, DiSPUTer, Università G. d'Annunzio, Campus Universitario di Madonna delle Piane – 66013 Chieti Scalo (CH), Italy
[2]Centro Ricerche Sismologiche, Istituto Nazionale di Oceanografia e Geofisica Sperimentale, Via Treviso, 55 – 33100 Udine, Italy and Borgo Grotta Gigante 42/C – 34010 Sgonico (TS), Italy
[3]Dipartimento della Protezione Civile, Via Vitorchiano, 2 – 00189 Roma, Italy

Received: 22 April 2013 – Accepted: 11 May 2013 – Published: 29 May 2013

Correspondence to: M. A. Romano (aromano@inogs.it)

Published by Copernicus Publications on behalf of the European Geosciences Union.

Abstract

Thanks to the installation of a temporary seismic network, a microseismicity study has been conducted in the Sulmona area (Abruzzo, Italy) with the aim of increasing the knowledge of seismogenic potential of existing active faults. In this work the first seven months (from 27 May to 31 December 2009) of recorded data have been analysed, over a total period of acquisition of about 30 months. Using a semi-automatic procedure, more than 800 local earthquakes has been detected, which highlight the background seismicity previously unknown. About 70 % of these events have been relocated using a 1-D velocity model estimated specifically for the Sulmona area. Phase readings quality is checked and discussed, with respect to weighting schemes used by location algorithms, too. The integration of temporary network data with all the other data available in the region enable us to obtain a statistically more robust dataset of earthquake locations. Both the final hypocentral solutions and phase pickings are released as online Supplement. Local magnitude values of the newly detected events ranges between −1.5 and 3.7 and the completeness magnitude for the Sulmona area during the study period is about 1.1. Duration magnitude coefficients have been estimated as well, for comparison/integration purposes. Local Gutenberg–Richter relationship, estimated from the microseismic data, features low *b* value, possibly suggesting that the Sulmona area is currently undergoing high stress, in agreement with other recent studies. The time-space distribution of the seismic activity with respect to the known active faults, as well the seismogenic layer thickness, are preliminarily investigated.

1 Introduction

A small, temporary seismometric network was deployed in the Sulmona area (central Italy, Fig. 1), during the seismic sequence which followed the devastating L'Aquila 2009 earthquake (6 April, M_w = 6.3, Chiaraluce et al., 2011; Lavecchia et al., 2012) with the

aim of increasing the knowledge of the seismogenic potential of existing active faults. This network, started on 27 May 2009 and it has been operating till 22 November 2011.

In the study area, some active faults are deemed capable of generating impending strong earthquakes by seismotectonic and seismic hazard studies (e.g. Boncio et al., 2004; Pace et al., 2006; Peruzza et al., 2011; De Natale et al., 2011). Nevertheless, during the last decades, the area has been almost completely aseismic, with only very minor and sporadic events (in a 20 km distance from Sulmona, $M = 3.7$ in October 1992, from CSI database, Castello et al., 2006, and $M = 3.8$ in March 2009, from ISIDE database, http://iside.rm.ingv.it/iside/standard/index.jsp). Low seismicity rates have also been found by the experiment performed through a temporary seismic network by Bagh et al. (2007). So the main goal of our temporary seismic survey was to highlight the occurrence of microseismicity not located by the Centralized National Seismic Network (RSNC) and the Abruzzo Seismic Network (RSA) during the post-seismic phase of the 2009 earthquake, and to recognize, if any, the space-time evolution of brittle deformations on the major faults of the area.

Reliability and accuracy in earthquake location are topics often neglected by earthquake catalogues; they are even less properly addressed when datasets come from temporary monitoring and earthquake distribution is used to support geological and structural interpretations. As discussed by Lee and Stewart (1981), locating local events accurately requires considerable efforts: good stations coordinates, reasonable crustal structure models, and reliable *P* and *S* readings are necessary but not sufficient conditions, as earthquake location is a nonlinear problem, and no "fool-proof" method exists if input data are not sufficient to constrain the problem (Husen and Hardebeck, 2010).

In this study, we analyse the first seven months of our seismic recordings (e.g. from 27 May to 31 December 2009). Data were acquired in continuous recording mode and processed off-line by an off-line semi-automatic procedure. In addition, they required ad hoc manual elaborations, as small local earthquakes were blurred in the ongoing intense activity of the L'Aquila seismic sequence, and the noise level at temporary sites

was high in some cases. Details on the detection/recognition procedures and data preprocessing are given in de Nardis et al. (2011). By integrating the data recorded by our temporary network with those retrieved from national and regional permanent networks (globally, 76 stations spread over an area of about 54 000 km^2), a final dataset of nearly 7000 phase readings and of about 800 located earthquakes was obtained.

This paper has two main goals: (1) to quantify the precision of phase readings and the accuracy of the locations, by exploring crustal velocity models and location algorithms, in order to release an original dataset of small magnitude earthquakes for the Sulmona area (provided as Supplement); (2) to estimate the completeness magnitude threshold and a reliable Gutenberg–Richter characterization of background seismicity of the study area, useful for seismic hazard purposes. Preliminary considerations on the seismogenic layer thickness and on the geometric links with the active faults pattern, based on the space-time distribution of microseismicity, are also advanced.

After presenting the temporary network in the tectonic framework of the Sulmona basin and surrounding areas (Sect. 2), we remind how we built our arrival times dataset and assessed its reliability in terms of uncertainty (Sect. 3). Then, we describe the procedure adopted for computing the local velocity model (Sect. 4), afterwards used in locating the recorded microseismicity (Sect. 5). Next, we focus on magnitude estimates, together with completeness threshold and Gutenberg–Richter parameters (Sect. 6). Finally, we discuss our results (Sect. 7).

2 The Sulmona temporary seismic survey in the seismotectonic context

On 27 May 2009 OGS (Istituto Nazionale di Oceanografia e di Geofisica Sperimentale) and GeosisLab (Laboratorio di Geodinamica e Sismogenesi, Chieti-Pescara University) installed a temporary seismometric network around the Sulmona basin (Fig. 1). This sector of the Central Apennines is adjacent to the area extensively covered by temporary stations, after the $M_w = 6.3$ L'Aquila earthquake (see for example Margheriti et al., 2011).

The Sulmona plain is one of the intermountain basins of the Abruzzo Apennines, east of the best-known Fucino basin (Fig. 1). It is filled by lacustrine continental deposits of Pleistocene-Holocene age and it is bounded eastward by the Morrone normal fault system. This system is characterized by two SW-dipping sub-parallel segments, extending for nearly 20 km along strike (Gori et al., 2011); the westernmost one shows a huge fault scarp at the contact between the carbonate bedrocks and slope deposits. It dislocates Late Pleistocene (related to the Last Glacial Maximum) alluvial fan and slope deposits and therefore is considered active (Gori et al., 2011). Southeastward, the Morrone fault system continues in the SSW-dipping Porrara normal fault, which runs about 18 km in NNW–SSE direction.

Other active extensional structures outcrop on the outskirts of the temporary network (Boncio et al., 2004; Galli et al., 2008; Lavecchia et al., 2012). They are the Paganica, the Middle Aterno Valley and the Conca Subaequana faults (n. 1, 2 and 3, respectively in Fig. 1), the Cinque Miglia fault (n. 4 in Fig. 1), the Fucino fault (n. 5 in Fig. 1) and its southward continuation into the Marsicano and Barrea faults (n. 6 and 7 in Fig. 1, respectively). Eastward of the Morrone-Porrara system, an impressive SW-dipping normal fault outcrops, known as "Caramanico Valley fault" (n. 8 in Fig. 1). The Quaternary activity of such structure, that bounds the Maiella Massif to the west, is still controversial in the literature (Ghisetti and Vezzani, 2002; Galadini and Messina, 2004).

Since early times in instrumental seismometry, the Fucino fault has been activated by the 1915 Avezzano earthquake (M_w = 7, Castenetto and Galadini, 1999), the Paganica fault by the 2009 L'Aquila earthquake (M_w = 6.3, Lavecchia et al., 2012) and the Barrea fault by the 1984 Val di Sangro earthquake (M_w = 5.4, Pace et al., 2002). No relevant instrumental earthquake is associated to the Morrone-Porrara alignment, which up to now has been only characterized by a very minor instrumental activity (Castello et al., 2006; ISIDE database – http://iside.rm.ingv.it/iside/standard/index.jsp; Bagh et al., 2007). Conversely, in historical times, the Sulmona plain has been the site of three destructive earthquakes, which occurred in the second century AD (M_w = 6.6,

Ceccaroni et al., 2009), in November 1706 (I_{max} = X/XI MCS, M_w = 6.8) and in September 1933 (I_{max} = IX MCS, M_w = 5.97) (Rovida et al., 2011; Guidoboni et al., 2007).

The OGS-GeosisLab temporary network, hereinafter referred as STN (Sulmona Temporary Network), consists of 6 mobile stations (SU network code in OASIS, the OGS Archive System of Instrumental Seismology, in the section "Sites", http://oasis.crs.inogs.it). These stations are integrated by 2 permanent ones (INTR and LPEL, IV network code in iside.rm.ingv.it/iside/standard/result.jsp?rst=1&page=STATIONS), belonging to the RSNC managed by INGV (Istituto Nazionale di Geofisica e Vulcanologia), for which continuous recordings were given as data exchange (see Table 1). The stations were located on both the hangingwall and the footwall of the Mt. Morrone and Mt. Porrara faults, with an inter-station distance of about 10 km (Fig. 1). Acquisition was set in continuous mode and the collected data were managed at the OGS by the Antelope system (BRTT, 2004). The network had been operating for 30 months, till the removal of all the mobile stations, occurred on 22 November 2011. Some STN stations were moved during the monitoring, for logistical reasons as well as in order to improve their performance. A full description of the sites, the equipment and their functioning is available at the OASIS website.

3 Waveform data processing, dataset of arrival times and uncertainty analysis

The STN seismological survey provided a huge amount of continuous seismic recording data (190 MB day^{-1}). However, the advantage of having a complete dataset collides with the drawback of needing an effective strategy in order to distinguish weak seismic signals from noise. Here we analyse only the data acquired during the first seven months, as they required peculiar data treatment due to the ongoing L'Aquila sequence, including manual operations hereinafter described. In this section we also refer to a preliminary location which represents an essential step of our work. Indeed it allowed the integration of our data with those from other existing networks, thanks to

the origin times, and the selection of good quality events through which we refine the velocity model.

3.1 Earthquake detection and preliminary location

The first step of this study is to recognize all the local seismicity, down to the weakest events, from the STN waveform data. In the period analysed in this experiment, the microseismicity detection was hampered by the ongoing L'Aquila seismic sequence, which started some months before the STN deployment and culminated with the deadly events of 6 April 2009, at 03:32 LT (M_w = 6.3, Chiaraluce et al., 2011) and by the high level noise of some stations due to the temporary installation of sensors. Therefore, in order to gain the maximum sensitivity a semi-automatic procedure has been applied, similar to that used by Garbin and Priolo (2013) for detecting small magnitude events in the Trento Province, which combines an automatic detection of all possible events and true event identification by visual inspection. This procedure is part of the general system implemented at CRS (Centro di Ricerche Sismologiche) for processing seismological data. It uses: (1) Antelope (BRTT, 2004) for acquiring/storing data, recognizing earthquakes automatically, and extracting earthquake waveforms; (2) a "pick-server" for phase picking and location, which are performed by Seisgram2K (Lomax, 2008) and Hypo71 (Lee and Lahr, 1975), respectively.

Earthquake recognition is performed by a sequence of two operations, i.e. trigger detection and trigger association, performed by Antelope through dbdetect and dbgrassoc functions, respectively. The first one uses a classical Short-Time Average/Long-Time Average (STA/LTA), while the second one declares an event when a group of detections is found to be compatible with the theoretical travel times for a unique source. There are several parameters controlling these algorithms (e.g. pass-band filtering) and the selection of their best combination is not trivial. False events (very frequent in noisy sites) increase with the choice of decreasing the STA/LTA threshold and using a low number of minimum stations, aimed at increasing the overall sensitivity of the automatic recognition. They can be identified and removed by human visual inspection.

Applied to the whole 7-months dataset, the automatic procedure extracted about 16 000 windows of signal which included teleseismic events, regional events (for example the L'Aquila aftershocks), local earthquakes (our target) and false events. All the windows were visually inspected, but only those containing local events (with time difference between *P* and *S* arrivals of less than about 3 s) were analysed. About 4700 phases were recognised and manually re-picked, identifying more than 800 microearthquakes. About 70 % of these events with more than 3 phases were preliminarily localized by using Hypo71 code (Lee and Lahr, 1975) and the velocity model used for ISIDE locations (Fig. 2).

The detection capabilities of the STN network obviously decrease by increasing the event-to-station distance. In fact, in a buffer zone corresponding to a 20 km distance from each STN station, the RSNC events (http://iside.rm.ingv.it/iside/standard/index.jsp) are 35 % of the ones localized by STN network (104 earthquakes versus 293), while they rise to 73 % (264 by RSNC versus 359 by STN) if the distance is set to 25 km. Several single station events were detected as well (e.g. in Fig. 3), but they may be located in terms of *S*–*P* distance only; most of them were recorded by SL06 station, at the southern tip of Mt. Porrara fault. In conclusion, as a result of the semi-automatic event recognition and of a more dense temporary network, this study provides a much detailed dataset for the Sulmona area than any other currently available for the Abruzzo. Bagh et al. (2007) detected in 18 months approximately the same number of events we did in 7 months, but referred to a wider area.

3.2 Improvement of phase readings

The parameters commonly used to evaluate the quality of the earthquake locations (number of phases, GAP, RMS, etc.) clearly indicate that the quality of our preliminary dataset, projected in the map of Fig. 2, is not enough for the purpose of seismotectonic analysis. With the aim of strengthening the earthquake catalogue, we integrated selectively the data, using other networks' data, and assessed the quality of phase readings and their overall reliability.

In particular, we included the data of 6 stations of the Abruzzo regional network (RSA, yellow triangles in Fig. 1) and of several stations of the national network (RSNC, blue triangles in the same figure), not acquired in real time during our experiment.

The considered RSA stations (AIE1, ORT1, PSC1, PTS1, SBP1 and SEM1) are the nearest to STN. Their recordings are discontinuous, as stations work on triggers (De Luca, 2011). Time coincidences between the origin time of our local earthquakes and automatic start time of RSA recordings have been searched. In 7 months, 37 triggered events correspond to earthquakes recognized by our network. From them, 115 *P* phases and 64 *S* phases (black sector in Fig. 4a) were manually picked.

Similarly, the integration of our dataset with other RSNC stations (INTR and LPEL are already part of the network experiment), has been carried out by verifying the correspondence of the origin times recognized by STN to those reported by ISIDE database in the same period. Those *P* and *S* arrival times were merged with ours with no further revision on phase picks. As a result, a total of 1251 *P* and 984 *S* arrival times from 60 RSNC stations (Fig. 1, blue triangles) were collected (yellow sector in Fig. 4a).

The complete dataset contains 6889 phases. It refers to 817 earthquakes, of which: 382 are identified by 1 or 2 STN stations, and located only if having at least 4 phase readings; 225 are located exclusively with STN stations; 210 are located with observations of STN, RSA and RSNC stations (Fig. 4a and b).

Uncertainty in phase readings is rarely declared in earthquake locations and catalogues, but this is an important element because location codes use this information in their weighting schemes. Formally, the estimate of measurement error has to be evaluated from a probabilistic point of view. According to this, the onset of a seismic phase should be described by a probabilistic function that reaches its maximum exactly at the arrival time of this phase, and the standard error corresponds to the standard deviation of the population. In this way information on statistical properties of the errors could be retrieved. More often, only a qualitative evaluation of the reading error is available, and the operator's choice cannot be evaluated rigorously. Reading errors are detected by a change in the amplitude and in the frequency content of the seismic

signal and are usually represented by a time window whose width is estimated by the operator and depends on the signal-to-noise ratio and the dominant frequency of the arriving phase (Husen and Hardebeck, 2010). Phase reading errors are then classified into categories which correspond to weight codes that are directly used by location algorithms. The larger the reading uncertainty is, the higher the Hypo71 weight code and the less this reading influences earthquake location. The mapping of reading errors into weights may be controlled by the seismologist, even though this is not always declared. For our case, the setting of weighting scheme tuned for performing locations with Hypo71 is shown in Table 2.

Some histograms of the phase reading errors are given in Fig. 5. The dataset contains readings from the STN and RSA networks obtained for this study manually, whereas we cannot retrieve the reading uncertainties for all the phases provided by the RSNC network, for which only the weight code and polarities, if any, are given. More than 90 % of the *P* and *S* original phases have a reading error less than or equal to 0.2 s (see Fig. 5a), while few outliers (7 for *P* phases, 1 for *S* phases), not represented in Fig. 5a, are in the range 0.4–0.54 s. Thus, none of our picks is given weight 4.

The permanent INTR station (see its location in Fig. 1) is the site with the greatest number of readings (Fig. 5b) related to local events. Also sites SL03/SLA3, SL05/SLA5 and SL06 are well represented (about or more than 300 *P*'s). Three stations (i.e., SL01, SL04 and LPEL) do have less data, because of some instrumental acquisition problems (for details, see de Nardis et al., 2011). Conversely, the small number of readings on the RSA stations is due to the triggered-mode acquisition, which cut off the detected earthquakes at a higher threshold.

The quality of pickings is statistically very good and similar for all the sites (Fig. 5c). For 11 over 16 stations (i.e. except for SLA3, SL04, SLA5, INTR and LPEL) both the median and 75th percentile is within 0.1 s; the 95th percentile is more scattered, although it never reaches 0.3 s. This is due to either the low sampling rate of the two

permanent stations – INTR and LPEL are often sampled at 20 Hz due to the lack of high-sampling channels – or the high noise level of the temporary stations.

As previously said, for the other RSNC stations we have only their weight code, with unknown weighting scheme. Therefore, we represent the histograms of weight codes for all the 60 stations, some of which sporadically enter in this dataset (Fig. 5d). Only 13 of them (CERA, CERT, FAGN, GIUL, GUAR, MIDA, POFI, PTQR, RNI2, SDI, VAGA, VCEL, VVLD – the location of the stations nearest to the STN network is reported in Fig. 1) are well represented, with weight equal to 0 (best quality) assigned to S phases. Only few observations are retrieved for the remaining, more distant stations, and they refer to events already listed in ISIDE.

Phase readings may be affected by systematic or random errors, however most of them can be identified and fixed through some conventional analyses. We checked the reliability and consistency of P and S phases by using the modified Wadati method (Chatelain, 1978), that compares the time difference of P and S phases recorded by couples of corresponding stations. Let be x_i and x_j the hypocentral distances of the k event at two stations (i, j), the following equations hold:

$$\mathrm{DT}_P = P_i - P_j = (x_i - x_j)/V_P \quad (1)$$

$$\mathrm{DT}_S = S_i - S_j = (x_i - x_j)/V_S \quad (2)$$

$$\frac{\mathrm{DT}_S}{\mathrm{DT}_P} = \frac{V_P}{V_S} \quad (3)$$

with V_P and V_S are the P and S wave velocity values, respectively. Figure 6a plots DT_S versus DT_P calculated for the original data and for all available pairs of STN stations, for a total of 4716 phases. At this step, outliers are identified and removed, either by correcting or erasing the reading. Figure 6b is thus obtained, and it takes into accounts 241 picks removed from the original dataset. Then, STN phase picks have been integrated with those read from RSA stations or provided by RSNC stations, for a total of 2414 additional phases. By refining and integrating the dataset of phases, the V_P/V_S estimated by ordinary least squares regression (equation coefficients and line,

with standard deviation, in red in Fig. 6) changes from 1.78 to 1.82. The orthogonal regression (in blue in Fig. 6) results in more stable values, all around 1.85. Since orthogonal regression is more adequate for data affected by errors on both the variables, we choose as final value the ratio V_P/V_S equal to 1.85, which is slightly higher than those obtained by other studies in the same region (1.83 by Bagh et al., 2007; 1.80 by De Luca et al., 2000; 1.77 by Boncio et al., 2009), but in agreement with the values estimated by Chiarabba et al. (2010) by local earthquake tomography, for which V_P/V_S exceeds 1.83.

4 Estimate of local velocity model

The systematic errors associated to the velocity model cannot be properly quantified, since earthquake hypocentres, earthquake origin times and seismic velocity structure (never exactly known) are intrinsically coupled (Husen and Hardebeck, 2010). Nevertheless, it is possible to estimate an optimized local velocity model which ensures the best tradeoffs between earthquake locations and crustal model in terms of travel time residuals. No specific velocity model to be used for event location is available for the Sulmona basin and surrounding areas. As the number of earthquakes of this study is too small for feeding a 3-D tomographic inversion, we adopt a 1-D velocity structure inversion approach using the well-known Velest code by Kissling et al. (1994).

4.1 Starting velocity models and selected dataset

In non-linear inversions which linearize the problem, it is crucial to define the initial guess accurately, since it affects strongly the final solution. Therefore, we compiled a collection of possible velocity models across the study area, taking into consideration and integrating the available seismological, geophysical and geological information on the crustal stratigraphy in terms of layers thickness and seismic wave velocity. As a result, twelve 1-D P wave velocity models with different structures were obtained and

taken as a starting point to calculate a reliable velocity model (Fig. 7 and references therein).

Five models (Fig. 7a–e) were derived from seismological data. Models a, b and c are local velocity models optimized for the intra-Apennine area. They were obtained by inverting P and S wave arrival times of local earthquakes recorded during a specific campaign (Bagh et al., 2007) or during L'Aquila 2009 seismic sequence (north-western sector of Fig. 1) (Chiarabba et al., 2009; Chiarabba et al., 2010). Model d is a regional velocity model valid for the whole Italian territory and used for the Italian Seismic Catalogue CSI (1981–2001) (Chiarabba et al., 2005) and model e was derived from it. Three models f–h were resulted from geophysical investigations, as deep seismic sounding data (DSS 11 by Scarascia et al., 1994; see the trace in Fig. 2), near vertical seismic reflection profile (CROP 11 by Patacca et al., 2008; see Fig. 2), also opportunely integrated with results obtained from teleseismic receiver functions (Di Luzio et al., 2009). Models i–l were built by integrating and correlating the stratigraphic layering as derived from the interpretation of the geological structure at depth along a crustal section across the Sulmona-Maiella area (Lavecchia and de Nardis, 2009). Note that different P wave velocity values have been attributed to the same layer by different authors (Patacca et al., 2008; Di Luzio et al., 2009; Barchi et al., 2003; Trippetta et al., 2013), and that the models often feature velocity inversions with depth (Fig. 7). Figure 8a emphasizes their great variability.

With the purpose to estimate the optimum 1-D velocity model, we selected the best constrained earthquakes, based on the quality of their preliminary locations. Since the study area is mainly characterized by sparse seismicity (except two relatively significant seismic sequences localized to NW and SW of the Sulmona basin, Fig. 2), we adopted two selection criteria. A more restrictive criterion was applied for the events located at the edge of the study area (107 events with RMS $\leq$ 0.5 s, GAP $\leq 180^{\circ}$, $N \geq 10$ phase readings with at least 4 clear S arrivals) and a less restrictive one for weaker earthquakes located within the local STN network (124 events with RMS $\leq$ 0.5 s, GAP $\leq 250^{\circ}$, $N \geq 6$ phase readings with at least 2 clear S arrivals). As

a result, a subset of 231 events (red dots in Fig. 2) was obtained, with P and S wave pickings having a mean reading uncertainty of 0.07 and 0.09 s respectively.

4.2 Minimum 1-D velocity model from travel times inversion

For the identification of the best 1-D velocity model, we considered a selected dataset of P and S arrival times (Fig. 2) and 12 different starting velocity models (Fig. 7). S wave readings were not inverted, but only included to better constrain the earthquake locations. A constant V_P/V_S ratio of 1.85 was imposed, as retrieved by the modified Wadati diagram discussed in Sect. 3.2.

The best 1-D velocity model was estimated by a trial and error process. First, we performed several inversions considering the collected velocity models, using identical input and control parameters and systematically verifying that the formal overdetermination factor (total number of observations/number of effective unknowns) of the inverse problem was at least greater than 1.5. Analysing the preliminary results, we noted that the output models were quite similar, in spite of the wide range of variability of the starting ones (Fig. 8a), implying a stable solution. Notwithstanding, we carried out further tests varying the control parameters. Afterwards, we created new velocity structures including phantom layers in each initial model. In fact, the Velest code does not automatically adjust layer thicknesses and the appropriate layering must be found performing trial inversions. Moreover, for each model we performed ten runs using final hypocenter locations, as initial parameters for the next one. Finally, we analysed the RMS (root mean square) misfit trend versus the number of iterations and chose the best model (the one corresponding to the minimum misfit of travel-time residuals) for each guess velocity structure.

The obtained results are summarized in the panels and in the table of Fig. 8. Specifically, Fig. 8b shows the range of variability (grey envelope) of the calculated 1-D velocity models with best misfit less than or equal to 0.1 s (value which is compatible with the uncertainty of the P and S wave pickings). The table in Fig. 8 reports the start and final travel-time residual for each of the 12 used models. The final velocity model (red line in

Fig. 8b) was chosen on the basis of goodness of the fit (0.110 s) and the consistency of the model with respect to local a priori geological and geophysical information (see references in Fig. 7) and taking into account worldwide compilations of the thickness and velocity structure of the crust in analogous tectonic provinces (Christensen and Mooney, 1995).

Three layers with velocity increasing from 5.1 to 5.7 km s^{-1} are distinguished from surface to a depth of 6 km, a fourth layer with velocity of 5.8 km s^{-1} is identified at depths between 6 and 13 km and a fifth layer with average velocity of 6.8 km s^{-1} characterises the interval between 13 and 27 km (Table 3); at higher depths, the velocity increases to an average value of 7.1 km s^{-1}.

Based on speculative correlations between the obtained velocity model and a suitable geological compositional layering for the study area, we advance the hypothesis that the uppermost three layers (average 5.6 km s^{-1}) may correspond to the upper sedimentary crust made of Jurassic-Paleocene carbonate sequence (limestone and dolomites) overlain by open-ramp carbonates and locally by Miocene turbidites.

The thick layer identified at depths between 6 and 13 km (average 5.8 km s^{-1}) may represent the oversimplification of a complex thrust zone where late Triassic evaporites (Anidriti di Burano formation) are tectonically interbedded with late Permian-Triassic quarzites and phyllites (Verrucano formation). We observe that the velocity inversions which would characterize such depth interval, mainly due to the presence of the very slow Verrucano formation (4.5 km s^{-1} in Patacca et al., 2008; Trippetta et al., 2013), do not result in the final velocity model, although they were introduced in several of the starting models in Fig. 7.

The sharp increase in the velocity gradient observed at 13 km might represent an increase in metamorphic grade, as well as a decrease in silica content, and can be interpreted as the top of the crystalline Palaeozoic basement of the middle crust. Another rather sharp increase in velocity is observed at a depth of 27 km. In agreement with the CROP 11 results, we might interpret it as the top of the lower crust, but evidently such

value is not well resolved, due to the lack of seismic activity beneath ∼24 km (see depth histogram in Fig. 8c).

It is important to specify that above optimized 1-D model is suitable for the most of the intra-mountain zone of the Abruzzo region, but station corrections need to be included when used on more extended areas. In fact, in Fig. 8d, it is evident that the station corrections are very low (less than 0.1 s) over the most of the study area, but they are slightly higher NNE-ward of Sulmona and eastward of the Maiella ridge, where the positive corrections reach 1 s, consistently with the presence of thick terrigenous deposits of the Plio-Pleistocene Adriatic foredeep.

5 Final earthquake locations

After the minimization of reading errors and the optimization of the velocity model for the study area we went to the final earthquake locations by using the code Hypoellipse (Lahr, 1980, 1984, 1999). It provides estimates of absolute position and origin time of all events. We recall that this program is the evolution of Hypo71 (used for preliminary locations in Fig. 2): it uses a weighted regression technique and introduces a new concept of error ellipsoid, representing Gaussian error distribution not necessarily aligned with latitude, longitude and depth axes, as Hypo71 does.

Very important parameters in Hypoellipse are the so-called WEIGHT OPTIONS that rule the influence of the uncertainty associated to each reading on the location process. In order to define the best values to assign to the 4 parameters involved in Hypoellipse weighting scheme (RESET TEST 29 and WEIGHT OPTIONS parameters) we adopt a procedure based on genetic algorithms (Bondar, 1994). Exploration of parameter space is driven so as to minimize the target function defined as a linear combination of the averages and standard deviations of *P* and *S* residuals returned by Hypoellipse over the whole earthquake dataset. The parameterization obtained is shown in Table 4.

Furthermore, time delays were associated to seismic stations, in order to consider both their elevation and possible local anomaly of velocity under them. These

corrections were automatically calculated, the former assuming a P wave velocity of 4 km s^{-1} in the sector of crust above the sea level, the latter setting the RELOCATE option and running through a number of iterations.

Finally, we located 535 earthquakes occurred from 27 May to 31 December 2009, 352 of which are of quality A, 32 of quality B, 16 of quality C and 135 of quality D. This means that their horizontal and vertical 68 % confidence interval (γ) is respectively: $\gamma \leq 1.34$ km for quality A, 1.34 km $< \gamma \leq 2.67$ km for quality B, 2.67 km $< \gamma \leq 5.35$ km for quality C, and $\gamma > 5.35$ for quality D (Lahr, 1999). Figure 9 shows the histograms which describe the locations of quality A events. More than 90 % of these hypocentral solutions features P and S residuals less than ±0.4 s (Fig. 9a, b), horizontal/vertical errors less than 1 km (Fig. 9c, d), and RMS less than or equal to 0.3 s (Fig. 9e). Only 60 % of the events has GAP less than or equal to 180° (Fig. 9f), i.e. their location is reliable. This result is satisfying if we consider that relatively few and small events were recorded within the STN, and among those outside only the strongest were located by using data from other networks (RSA and RSNC), with the advantage of reducing GAP. Moreover, thanks to the enrichment of our dataset, more than 30 % of locations are estimated using more than 16 phases (Fig. 9g). In 45 % of the cases the minimum distance between the hypocentre and the closest station is less than or equal to 5 km, and in about 30 % it is less than or equal to 10 km (Fig. 9h), i.e. to the inter-STN station distance.

Final earthquake locations (Fig. 10a), obtained after building a good quality dataset and estimating the local velocity model, improve the preliminary ones (Fig. 2). Indeed background seismicity, initially widespread over the area, now tends to cluster close to known tectonic structures or, in any case, to focus in restricted areas.

6 Magnitude, completeness and local G–R relationship

Magnitudes are computed for the final hypocentral locations previously described. We estimated them in terms of both signal amplitude (M_L) and duration (M_D).

Local magnitude (M_L) is obtained by applying Antelope's dbampmag (BRTT, 2004) and using the Hutton and Boore's attenuation law (1987). In order to preserve compatibility with older magnitude estimates, M_L is calculated as the mean of the magnitude estimated for each station, where the magnitude at each station is calculated from the mean of the waveform amplitude of the two horizontal components (Bormann, 2002). Single station compensation coefficients have been estimated and applied, too. They exhibit randomly distributed values smaller than ±0.2, except for stations SLA3 and SLA5 (respectively +0.42 and +0.30), which were repositioned after logistic problems to the original sites.

Local magnitudes, estimated in this study, range from −1.5 to 3.7 (Fig. 11a). The 93 % of events has M_L between −0.1 and 2, while the remaining 7 % is distributed as follows: the 2 % has $M_L < -0.1$, the 4 % has M_L between 2 and 3 and only the 1 % has $M_L > 3$. Furthermore eight of 535 earthquakes lack amplitude data, for noise problems.

By comparing our M_L estimates to those derived from ISIDE for about 200 events common to both networks (Fig. 11b), it comes out that the M_L of this study is higher than that estimated by ISIDE for a value of about 0.15.

As a shortcut to local magnitude estimation, we calculate the duration magnitude (M_D), as well. We used the following simplified formula:

$$M_D = a_1 + a_2 \log(\tau) \quad (4)$$

where τ is the signal duration in seconds; the distance term is not considered as it turned out to be negligible. Due to the presence of noise, the signal duration has not been read and therefore M_D has not been estimated for 207 of 535 events. For the remaining 328 earthquakes M_D values range from −0.9 and 3.7.

Mean station coefficients have been estimated by calibrating M_D against M_L (Fig. 11c) by applying ordinary least squares and orthogonal regressions. Duration magnitudes are then obtained by entering the coefficients of the orthogonal regression into the pertinent RESET TEST values of Hypoellipse (i.e. (31) equal to −3.2843; (32) equal to 3.3129; (33), (40), and (43) set to zero). It can be seen from Fig. 11c that the

orthogonal regression represents the highest M_L fairly well, even if the data are quite dispersed.

Finally, a statistical analysis of magnitude versus event frequency relationship and an estimation of the completeness magnitude inferred on the Gutenberg–Richter (1956) model is carried out by using Zmap software (Wiemer, 2001). The result is shown in Fig. 11d. The completeness magnitude (M_c) of our relocated dataset (27 May to 31 December 2009) is 1.1. Note that the coefficients of the Gutenberg–Richter relationship, i.e. the annual *a* value (3.49) and *b* value (0.85), are not representative of the Sulmona basin only, as part of the L'Aquila seismic sequence and a bulk of earthquakes in the SW Sora region (see Fig. 10a) fall inside the relocated events. If we select the events spatially in a buffer zone of 20 km around the STN stations, thus selecting earthquakes where the detection capabilities of the temporary network are at the best, we obtain a equal to 3.11, b to 0.71 and M_c to 0.72.

7 Discussion and conclusions

The present paper aims at improving the knowledge of the background seismic activity in the Sulmona basin, an extensional active area of Central Apennines ascribed of strong seismic hazard (Pace et al., 2006), but substantially aseismic since instrumental times (Bagh et al., 2007; Boncio et al., 2009). Thanks to the deployment of a temporary seismic network and to the analysis of the first seven month of recorded data, properly processed, we have obtained a detailed picture of the microseismicity not revealed until now by either existing permanent networks (ISIDE database; De Luca, 2011) or other similar experiments performed in the past (Bagh et al., 2007). The meta-data gathered during this period were somehow peculiar and time-demanding for what concerns signal treatment, due to the ongoing seismic activity in the L'Aquila area. The processing combines an automatic detection procedure with operator-assisted selection of windows, and a fully manual readings of waveforms on local events (chosen on *S*–*P* time delays). This approach has proved to be very effective, even though quite

time consuming, in identifying even very small earthquakes, such as local events with $M_L < -1$ recorded just by one or two stations. The integration of the STN recordings with the data gathered by regional and national permanent networks (RSA and RSNC) enriched and strengthened the location quality of the strongest earthquakes. As phases are homogeneously read, and accuracy is clearly stated, a well-constrained 1-D velocity model of the Sulmona area and a reliable V_P/V_S ratio of 1.85 was obtained, which guarantees accurate earthquake locations and may be useful for forthcoming studies in the area.

In this paper, an on line catalogue of the analysed earthquakes is compiled and released as Supplement together with the phase pickings. The catalogue contains: the origin times and the hypocentral coordinates of located earthquakes; all the parameters useful to establish the quality of their locations (RMS, GAP, number of phases used, minimum distance, dimension and orientation of error ellipsoids); the magnitude estimate, both local and duration if possible. The catalogue includes 535 events, that are about 60 % more than the ones reported in the national ISIDE database. An additional set of 282 not located earthquakes is given by phase readings only, for possible further analyses. The quality location of nearly 66 % of the located events is A, nevertheless their very small magnitude. Indeed the 99 % of located seismicity is represented by ultramicro- ($M < 1$) and micro-earthquakes ($1 \leq M_L < 3$), while only the 1 % is represented by small earthquakes $M_L \geq 3$ (Hagiwara, 1964) (Fig. 11a). The completeness magnitude M_c, based on local magnitude estimates, is well constrained and reaches the value of 1.1 for the whole dataset of located events. It lowers to 0.7 if only the area strictly pertaining to the STN stations is considered. This low value of M_c confirms that the adopted semi-automatic procedure based on automatic detection of events and manual picking is very effective for investigating the microseismicity.

A well constrained G–R slope was estimated from the microseimic data (Fig. 11d). We observe that the productivity rates shown by the *a* value are nearly constant, if normalized to the area shaped on temporary stations coverage, whereas the *b* value decreases from 0.85 to 0.71. Following results from recent studies that consider the

b value as a stress indicator (Gulia and Wiemer, 2010), we advance the hypothesis that the Sulmona area might be more stressed than the surroundings. Whether the obtained G–R values can be considered representative of stationary background conditions or might have been influenced by static/dynamic stress changes induced by the main L'Aquila earthquakes is questionable. Evidence of stress loading in the Sulmona basinal area induced not only by the L'Aquila 2009 earthquake, in the north, but also by the 1984 Val di Sangro earthquake in the south, were pointed out by De Natale et al. (2011) based on the results from coseismic Coulomb stress change studies.

A seismotectonic analysis of the geometric and kinematic relationship between the Sulmona microearthquake activity and the active faults in the area are beyond the aim of this paper. Nevertheless some preliminary observations on the space-time distribution of identified clusters of seismic activity and on the overall seismogenic thickness can be advanced. We observe that the background seismicity is not uniformly distributed in the study area, but rather clustered in specific zones, mainly close to known active faults (Fig. 10a). A prevailing activity is observed at the northwestern corner of the study area, which coincides with the southern end of the Paganica seismogenic source responsible for the 2009 L'Aquila earthquake (M_w = 6.3, Lavecchia et al., 2012); conversely the area of the Sulmona plain remained almost completely aseismic during all the observation time.

The temporal evolution of the recorded seismic activity, schematized as cumulative number of events versus time (Fig. 10b), shows a sharp decrease in seismic rate at the end of June, e.g. after near one month of registration and nearly two months the 6 April 2009 earthquake (M_w = 6.3). The remaining portion of the cumulative slopes shows other jumps, corresponding to local and short lasting increases in the seismic activity. Three swarms were recorded from 2 to 22 June. They occurred within the hangingwall of the Porrara fault (cluster A, with M_L up to 1.7, and C1, with M_L up to 2.5, in Fig. 10a), and within the footwall of the Morrone fault (cluster B, with M_L up to 1.2, and C2 with M_L up to 0.9 in Fig. 10a), near the southern and the northern tip ends of the Morrone-Porrara extensional alignment, respectively.

On 4 August the area near Roccasicura (Molise Region) sited along the SSE-ward prosecution of the Morrone-Porrara extensional alignment, was affected by a little swarm of ten earthquakes (cluster D, in Fig. 10a), at depths between 13 and 17 km, with two larger events of M_L = 3.5 and 3.6 (Fig. 10a). Two other swarms occurred at the beginning of October 2009. The first one (12 events between 4 and 5 October, with M_L up to 1.7; cluster E in Fig. 10a) was located at the hangingwall of Marsicano fault at depths of 6–12 km; the second one (80 events between 6 and 8 October, with M_L up to 3.6 as in ISIDE; cluster F in Fig. 10a) nucleated near Sora (Lazio Region) at depth of 6 to 14 km. Finally, on 19–20 November, another increase of seismicity, with spatial distribution similar to that of the late June activity, was recorded at the footwall of the Morrone fault (cluster G1 with M_L up to 1.6 in Fig. 10a) and at the hangingwall of the Porrara fault (cluster G2 with M_L up to 2.9 in Fig. 10a).

We also performed a preliminarily evaluation on the Sulmona seismogenic layer, defined as the depth layer that releases the largest number of earthquakes (i.e. 95 % of the seismicity – D95, Williams, 1996; Fernandez-Ibañez and Soto, 2008). The frequency-depth histogram of Fig. 9i which was only built on the basis of quality A earthquakes, shows that 7 % of the events were shallower than 5 km, 24 % occurred at depths between 5 and 9 km, 42 % concentrated in the 9–12 km depth interval, 22 % between 12 and 17 km and the remaining 5 % between 17 and 21 km. Therefore, the base of the seismogenic layer which releases 95 % of the seismicity is located at a depth of 17 km. A thickness of 12 km (from 5 to 17 km) may be assumed for the brittle layer, considered as the layer within which nearly 90 % of the seismicity occurs. These values are in agreement with other independent estimates, done in this sector of the Apennines, based on rheological evaluations (Boncio et al., 2009).

To conclude, we point out that the detailed analysis and quality study performed in this paper, to obtain a low-magnitude complete catalogue for the Sulmona area, confirm and further highlight the low activity seismicity rate characterizing the study area with important implications in seismic hazard evaluation.

Supplementary material related to this article is available online at: http://www.nat-hazards-earth-syst-sci-discuss.net/1/2353/2013/nhessd-1-2353-2013-supplement.zip.

Acknowledgements. This project is self-financed by OGS (CRS Department) and the University of Chieti (GeosisLab, head Giusy Lavecchia). We thank all Mayors of the municipalities involved; Silvano Agostini of the Regional board of the Ministry of Cultural Heritage and Environmental Conservation; the DPC – Civil Protection Department and the INGV – National Institute of Geophysics and Volcanology for data exchange. Special thanks go to Gaetano De Luca (INGV) for his great job in gathering and providing us the data recorded by the Abruzzo Seismic Network (RSA) and Francesco Mele (INGV) for his precious help in retrieving the phase picking of the National Seismic Network (RSNC).

References

Bagh, S., Chiaraluce, L., De Gori, P., Moretti, M., Govoni, A., Chiarabba, C., Di Bartolomeo, P., and Romanelli, M.: Background seismicity in the Central Apennines of Italy: the Abruzzo region case study, Tectonophysics, 444, 80–92, 2007.

Barchi, M., Minelli, G., Magnani, B., and Mazzotti, A.: Line CROP 03: Northern Apennines, Memorie Descrittive della Carta Geologica d'Italia, LXII, 127–136, 2003.

Boncio, P., Lavecchia, G., and Pace, B.: Defining a model of 3-D seismogenic sources for Seismic Hazard Assessment applications: the case of Central Apennines (Italy), J. Seismol., 8, 407–425, 2004.

Boncio, P., Tinari, D. P., Lavecchia, G., Visini, F., and Milana, G.: The instrumental seismicity of the Abruzzo Region in Central Italy (1981–2003): seismotectonic implications, B. Soc. Geol. Ital., 128, 367–380, 2009.

Bondar, I.: Hypocentre determination of local earthquakes using genetic algorithm, Acta Geod. Geophys. Hu., 29, 39–56, 1994.

Bormann, P.: New Manual of Seismological Observatory Practice, GeoForschungsZentrum, Potsdam, 2002.

BRTT (Boulder Real Time Tecnology): Evolution of the Commercial ANTELOPE Software, Open file Report, available at: http://www.brtt.com/docs/evolution.pdf (last access: 22 April 2013), 2004.

Castello, B., Selvaggi, G., Chiarabba, C., and Amato, A.: CSI – Catalogo della sismicità italiana 1981–2002, versione 1.1, INGV-CNT, Roma, available at: http://csi.rm.ingv.it/ (last access: 22 April 2013), 2006.

Castenetto, S. and Galadini, F. (Eds.): 13 gennaio 1915, Il terremoto nella Marsica, Istituto Poligrafico e Zecca dello Stato, Roma, 788 pp., 1999.

Ceccaroni, E., Ameri, G., Gómez Capera, A. A., and Galadini F.: The 2nd century AD earthquake in Central Italy: archaeo-seismological data and seismotectonic implications, Nat. Hazards, 50, 335–359, doi:10.1007/s11069-009-9343-x, 2009.

Chatelain, J.: Étude fine de la sismicité en zone de collision continentale à l'aide d'un réseau de stations portables: la région Hindu–Kush–Pamir, Ph.D. thesis, Université Paul Sabatier, Toulouse, 1978.

Chiarabba, C., Jovane, L., and Di Stefano, R.: A new look to the Italian seismicity: seismotectonic inference, Tectonophysics, 395, 251–268, 2005.

Chiarabba, C., Amato, A., Anselmi, M., Baccheschi, P., Bianchi, I., Cattaneo, M., Cecere, G., Chiaraluce, L., Ciaccio, M. G., De Gori, P., De Luca, G., Di Bona, M., Di Stefano, R., Faenza, L., Govoni, A., Improta, L., Lucente, F. P., Marchetti, A., Margheriti, L., Mele, F., Michelini, A., Monachesi, G., Moretti, M., Pastori, M., Piana Agostinetti, N., Piccinini, D., Roselli, P., Seccia, D., and Valoroso, L.: The 2009 L'Aquila (central Italy) MW6.3 earthquake: main shock and aftershocks, Geophys. Res. Lett., 36, L18308, doi:10.1029/2009GL039627, 2009.

Chiarabba, C., Bagh, S., Bianchi, I., De Gori, P., and Barchi, M.: Deep structural heterogeneities and the tectonic evolution of the Abruzzi region (Central Apennines, Italy) revealed by microseismicity, seismic tomography, and teleseismic receiver functions, Earth Planet. Sc. Lett., 295, 462–476, 2010.

Chiaraluce, L., Chiarabba, C., De Gori, P., Di Stefano, R., Improta, L., Piccinini, D., Schlagenhauf, A., Traversa, P., Valoroso, L., and Voisin, C.: The 2009 L'Aquila (central Italy) seismic sequence, B. Geofis. Teor. Appl., 52, 367–387, doi:10.4430/bgta0019, 2011.

Christensen, N. I. and Mooney, W. D.: Seismic velocity structure and composition of the continental crust: A global view, J. Geophys. Res., 100, 9761–9788, 1995.

De Luca, G.: La Rete Sismica regionale Abruzzo e sua integrazione con la RSN, in: Riassunti estesi del I Workshop Tecnico "Monitoraggio sismico del territorio nazionale: stato dell'arte e sviluppo delle reti di monitoraggio sismico", INGV, Roma, 22–23, 2011.

De Luca, G., Scarpa, R., Filippi, L., Gorini, A., Marcucci, S., Marsan, P., Milana, G., and Zambonelli, E.: A detailed analysis of two seismic sequences in Abruzzo, Central Apennines, Italy, J. Seismol., 4, 1–21, 2000.

de Nardis, R., Garbin, M., Lavecchia, G., Pace, B., Peruzza, L., Priolo, E., Romanelli, M., Romano, M. A., Visini, F., and Vuan, A.: A temporary seismic monitoring of the Sulmona area (Abruzzo, Italy) for seismotectonic purposes, B. Geofis. Teor. Appl., 52, 651–666, 2011.

De Natale, G., Crippa, B., Troise, C., and Pingue, F.: Abruzzo, Italy, Earthquakes of April 2009: heterogeneous fault-slip models and stress transfer from accurate inversion of ENVISAT-InSAR data, B. Seismol. Soc. Am., 101, 2340–2354, doi:10.1785/0120100220, 2011.

Di Luzio, E., Mele, G., Tiberti, M. M., Cavinato, G. P., and Parotto, M.: Moho deepening and shallow upper crustal delamination beneath the central Apennines, Earth Planet. Sc. Lett., 280, 1–12, 2009.

Fernandez-Ibañez, F. and Soto, J. I.: Crustal rheology and seismicity in the Gibraltar Arc (western Mediterranean), Tectonics, 27, 1–18, 2008.

Galadini, F. and Messina, P.: Early-Middle Pleistocene eastward migration of the Abruzzi Apennine (central Italy) extensional domain, J. Geodyn., 37, 57–81, 2004.

Galli, P., Galadini, F., and Pantosti, D.: Twenty years of paleoseismology in Italy, Earth-Sci. Rev., 88, 89–117, 2008.

Garbin, M. and Priolo, E.: Seismic event recognition in the Trentino area (Italy): performance analysis of a new semi-automatic system, Seismol. Res. Lett., 84, 65–74, doi:10.1785/0220120025, 2013.

Ghisetti, F. and Vezzani, L.: Normal faulting, extension and uplift in the outer thrust belt of the central Apennines (Italy): role of the Caramanico fault, Basin Res., 14, 225–236, 2002.

Gori, S., Giaccio, B., Galadini, F., Falcucci, E., Messina, P., Sposato, A., and Dramis, F.: Active normal faulting along the Mt. Morrone south-western slopes (central Apennines, Italy), Int. J. Earth Sci., 100, 157–171, 2011.

Guidoboni, E., Ferrari, G., Mariotti, D., Comastri, A., Tarabusi, G., and Valensise, G.: CFTI4Med, Catalogue of Strong Earthquakes in Italy (461 B.C.–1997) and Mediterranean Area (760 B.C.–1500), available at: http://storing.ingv.it/cfti4med/ (last access: 22 April 2013), 2007.

Gulia, L. and Wiemer, S.: The influence of tectonic regimes on the earthquake size distribution: a case study for Italy, Geophys. Res. Lett., 37, L10305, doi:10.1029/2010GL043066, 2010.

Gutenberg, B. and Richter, C. F.: Earthquake magnitude, intensity, energy, and acceleration (second paper), B. Seismol. Soc. Am., 46, 138–154, 1956.

Hagiwara, T.: Brief description of the project proposed by the earthquake prediction research group of Japan, in: Proc. US – Japan Conf. Res. Relat. Earthquake Prediction Probl., Earthquake Research Institute, Tokyo, 10–12, 1964.

Husen, S. and Hardebeck, J. L.: Earthquake location accuracy, Community Online Resource for Statistical Seismicity Analysis, doi:10.5078/corssa-55815573, available at: http://www.corssa.org (last access: 22 April 2013), 2010.

Hutton, L. K. and Boore, D. M.: The M_L scale in Southern California, B. Seismol. Soc. Am., 77, 2074–2094, 1987.

ISIDe Working Group (INGV): Italian Seismological Instrumental and parametric database, available at: http://iside.rm.ingv.it (last access: 22 April 2013), 2010.

Kissling, E., Ellsworth, W. L., Eberhart-Phillips, D., and Kradolfer, U.: Initial reference models in local earthquake tomography, J. Geophys. Res., 99, 19635–19646, 1994.

Lahr, J. C.: HYPOELLIPSE/MULTICS: A Computer Program for Determining Local Earthquake Hypocentral Parameters, Magnitude and First-Motion Pattern, US Geological Survey Open-File Report 80-59, 59 pp., 1980.

Lahr, J. C.: HYPOELLIPSE/VAX: A Computer Program for Determining Local Earthquake Hypocentral Parameters, Magnitude and First-Motion Pattern, US Geological Survey Open-File Report 84-519, 76 pp., 1984.

Lahr, J. C.: HYPOELLIPSE: A Computer Program for Determining Local Earthquake Hypocentral Parameters, Magnitude and First-Motion Pattern (Y2K Compliant Version), Version 1.0., US Geological Survey Open-File Report 99-23, On-Line Edition, 1999.

Lavecchia, G. and de Nardis, R.: Seismogenic sources of major earthquakes of the Maiella area (Central Italy): constraints from macroseismic field simultaions and regional seimotectonics, UR 4.01-S1–29, Poster at the INGV-DPC meeting, Rome, November, 2009.

Lavecchia, G., Ferrarini, F., Brozzetti, F., de Nardis, R., Boncio, P., and Chiaraluce, L.: From surface geology to aftershock analysis: constraints on the geometry of the L'Aquila 2009 seismogenic fault system, Ital. J. Geosci., 131, 330–347, doi:10.3301/IJG.2012.24, 2012.

Lee, W. H. K. and Lahr, J. C.: HYP071 (Revised): A Computer Program for Determining Hypocenter, Magnitude and First-motion Pattern of Local Earthquakes, US Geological Survey Open File Report 75–311, 1975.

Lee, W. H. K. and Stewart, S. W.: Principles and Applications of Microearthquake Networks, Academic Press, New York, 293 pp., 1981.

Lomax, A.: SeisGram2K (5.3), Mouans-Sartoux, http://alomax.free.fr/seisgram/SeisGram2K.html (last access: 22 April 2013), 2008.

Margheriti, L., Chiaraluce, L., Voisin, C., Cultrera, G., Govoni, A., Moretti, M., Bordoni, P., Luzi, L., Azzara, R., Valoroso, L., Di Stefano, R., Mariscal, A., Improta, L., Pacor, F., Milana, G., Mucciarelli, M., Parolai, S., Amato, A., Chiarabba, C., De Gori, P., Lucente, F. P., Di Bona, M., Pignone, M., Cecere, G., Criscuoli, F., Delladio, A., Lauciani, V., Mazza, S., Di Giulio, G., Cara, F., Augliera, P., Massa, M., D'Alema, E., Marzorati, S., Sobiesiak, M., Strollo, A., Duval, A. M., Dominique, P., Delouis, B., Paul, A., Husen, S., and Selvaggi, G.: Rapid response seismic networks in Europe: lessons learnt from the L'Aquila earthquake emergency, Ann. Geophys., 54, 392–399, doi:10.4401/ag-4953, 2011.

Pace, B., Boncio, P., and Lavecchia, G.: The 1984 Abruzzo earthquake: an example of seismogenic process controlled by interaction between differently oriented syn-kinematic faults, Tectonophysics, 350, 237–254, 2002.

Pace, B., Peruzza, L., Lavecchia, G., and Boncio, P.: Layered seismogenic source model and probabilistic seismic-hazard analyses in central italy, B. Seismol. Soc. Am., 96, 107–132, 2006.

Patacca, E., Scandone, P., Di Luzio, E., Cavinato, G. P., and Parotto, M.: Structural architecture of the central Apennines: interpretation of the CROP 11 seismic profile from the Adriatic coast to the orographic divide, Tectonics, 27, TC3006, doi:10.1029/2005TC001917, 2008.

Peruzza, L., Pace, B., and Visini, F.: Fault-based earthquake rupture forecast in central Italy: remarks after the l'aquila M_w 6.3 Event, B. Seismol. Soc. Am., 101, 404–412, doi:10.1785/0120090276, 2011.

Rovida, A., Camassi, R., Gasperini, P., and Stucchi, M. (Eds).: CPTI11, la versione 2011 del Catalogo Parametrico dei Terremoti Italiani, Milano, Bologna, available at: http://emidius.mi.ingv.it/CPTI11/ (last access: 22 April 2013), 2011.

Scarascia, S., Lozej, A., and Cassinis, R.: Crustal structures of the Ligurian, Tyrrhenian and Ionian seas and adjacent onshore areas interpreted from wide angle seismic profiles, B. Geofis. Teor. Appl., 36, 5–19, 1994.

Trippetta, F., Collettini, C., Barchi, M. R., Lupattelli, A., and Mirabella, F.: A multidisciplinary study of a natural example of CO_2 geological storage in central Italy, Int. J. Greenh. Gas Con., 12, 72–83, 2013.

Wiemer, S.: A software package to analyze seismicity: ZMAP, Seismol. Res. Lett., 72, 373–382, available at: http://www.earthquake.ethz.ch/software/zmap (last access: 22 April 2013), 2001.

Williams, C. F.: Temperature and the seismic/aseismic transition: observations from the 1992 Landers earthquake, Geophys. Res. Lett., 23, 2029–2032, 1996.

Working Group OASIS: The OGS Archive System of Instrumental Seismology, http://oasis.crs.inogs.it (last access: 22 April 2013), 2011.

Table 1. Main characteristics of the Sulmona Temporary Network: data taken from OGS and INGV sites archives. SLA is the identification code of relocated SL0 stations.

Station Code/ Network	Municipality (PROVINCE)	Lon (DD)	Lat (DD)	Elevation (m a.s.l.)	Date ON/OFF	Sensor/ Data Logger
SL01/SU	Goriano Sicoli (L'AQUILA)	13.7827	42.0835	769	27 May 2009/ 24 Mar 2010	Lennartz3Dlite/ RefTek RT 130
SL02/SU	Popoli (PESCARA)	13.8539	42.1745	684	27 May 2009/ 22 Nov 2011	CMG-40, FBA ES-T/ RefTek RT 130
SL03/SU	Sulmona (L'AQUILA)	13.9336	42.0890	484	27 May 2009/ 1 Oct 2009	Lennartz -3Dlite/ RefTek RT 130
SLA3/SU	Sulmona (L'AQUILA)	13.9342	42.0895	523	1 Oct 2009/ 22 Nov 2011	Lennartz -3Dlite/ RefTek RT 130
SL04/SU	Pacentro (L'AQUILA)	14.0296	42.0730	1281	26 May 2009/ 22 Nov 2011	Lennartz -3Dlite/ RefTek RT 130
SL05/SU	Rocca Pia (L'AQUILA)	13.9787	41.9371	1067	26 May 2009/ 1 Oct 2009	Lennartz -3Dlite/ RefTek RT 130
SLA5/SU	Rocca Pia (L'AQUILA)	13.9773	41.9325	1108	1 Oct 2009/ 22 Nov 2011	Lennartz -3Dlite/ RefTek RT 130
SL06/SU	Palena (CHIETI)	14.1127	41.9083	1279	26 May 2009/ 24 Mar 2010	CMG-40, FBA ES-T/ RefTek RT 130
INTR/IV	Introdacqua (L'AQUILA)	13.9046	42.0115	924	9 Mar 2003/ –	Trillium 40S/ Trident-FS-16-VPP SG-1
LPEL/IV	Lama dei Peligni (CHIETI)	14.1832	42.0468	760	11 Apr 2008/ –	Trillium 40S/ GAIA2-FS-16-VPP

Table 2. Weighting scheme adopted in the preliminary locations performed by using Hypo71 (Lee and Lahr, 1975).

Weight Code	Reading Error
0	< 0.01 s
1	[0.01–0.04 s)
2	[0.04–0.20 s)
3	[0.20–1.00 s)
4	≥ 1.00 s

Table 3. The best 1-D velocity model estimated for the Sulmona area and its inferred composition layering.

	Lithostratigraphy	Depth interval (km)	Velocity ($km\,s^{-1}$)
UPPER CRUST	Miocene turbidites and Jurassic-Paleocene carbonates	0–2 2–4 4–6	5.1 5.4 5.7
	Triassic evaporites and Late Permian-Triassic quarzites and phyllites	6–13	5.8
MIDDLE CRUST	Crystalline Paleozoic basement	13–27	6.8
LOWER CRUST	Mafic granulite	27–38	7.1
MANTLE	Peridotite	> 38	8.0

Table 4. Weighting scheme adopted in the locations performed by using Hypoellipse. Parameter labelled with [a] represents RESET TEST 29. Parameters labelled with [b] represent WEIGHT OPTIONS. Refer to Hypoellipse User's Guide (Lahr, 1999) for details.

Weight code	Standard error	Standard error relative to readings with weight code zero	Computed weight
0	0.0350 s[a]	1	1
1	0.0455 s	1.3[b]	1/1.69
2	0.0700 s	2.0[b]	1/4
3	0.4375 s	12.50[b]	1/156.25
4	INFINITE	INFINITE	0

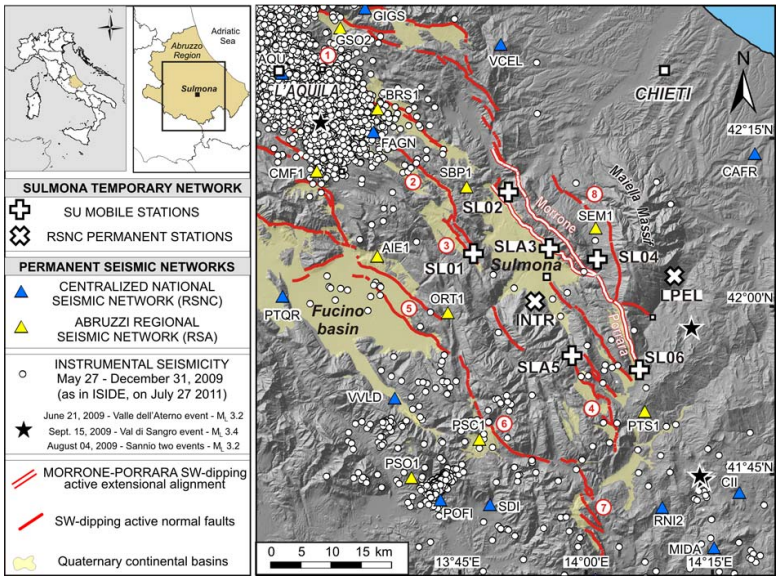

Fig. 1. Station locations and epicentral distribution of seismic events recorded by the INGV National Seismic Network (RSNC, http://iside.rm.ingv.it/iside/standard/index.jsp) in the Sulmona area (Abruzzo region) during the period 27 May–31 December 2009. The black stars indicate the epicentres of the strongest events located in this study: from north to south, they are listed in the legend. SU stations are labelled by plusses, crosses show the two permanent stations of the RSNC acquired in continuous and treated off-line as data exchange. Selected data of other permanent stations of the RNSC and of the Abruzzi Regional Seismic Network (RSA, see De Luca, 2011) were used in this study and are marked by blue and yellow triangles, respectively. The red numbers correspond to fault systems cited in the text.

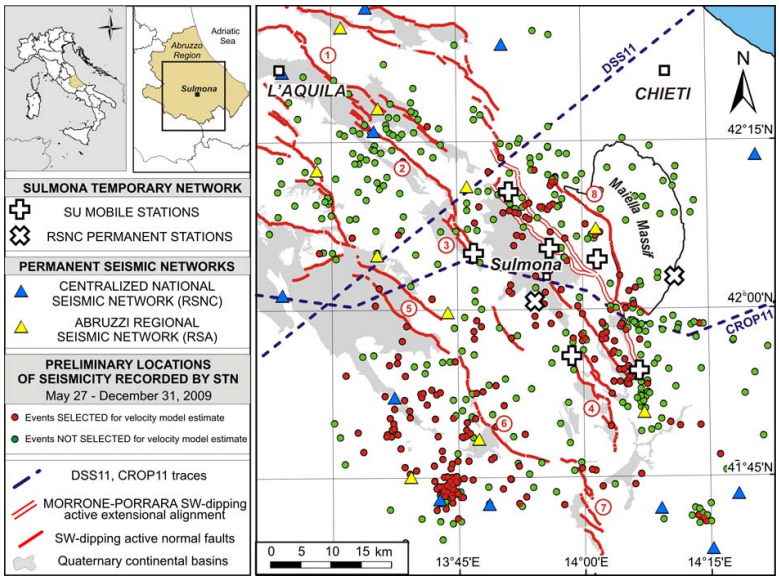

Fig. 2. Preliminary locations of earthquakes from 27 May to 31 December 2009, obtained with Hypo71 (Lee and Lahr, 1975) and the ISIDE velocity model.

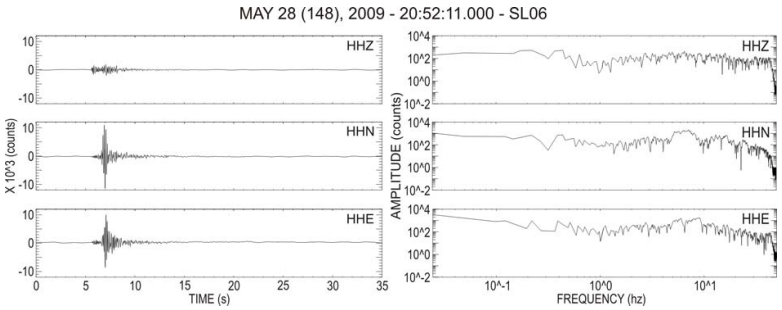

Fig. 3. Seismograms and amplitude spectra of a typical single station event recorded by three-component station SL06. Date and time above refer to starting point of the seismic trace. For this event, a source-station distance of about 8 km can be estimated from *S*–*P* time of 1 s.

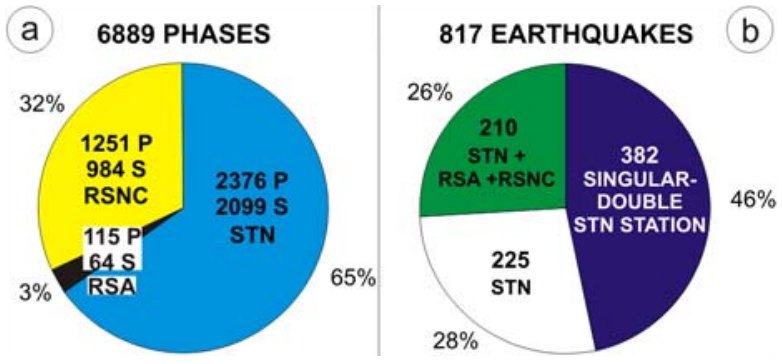

Fig. 4. Meta-data obtained by the STN network in the first 7 months. **(a)** Total number of seismic phases obtained after the integration of STN data with those from regional (RSA) and national (RSNC) permanent networks. **(b)** Total number of earthquakes representing our complete dataset.

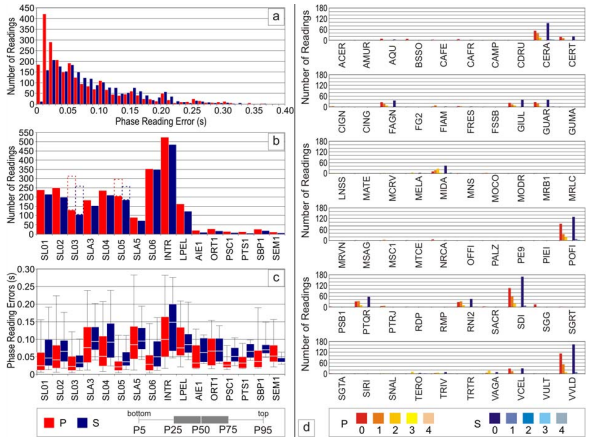

Fig. 5. Left: accuracy of pickings for all the phases read in this study. Period from 27 May to 31 December 2009. Right: weight code distribution for the RSNC stations used. **(a)** Number of *P* and *S* phases (in red and blue respectively) versus reading errors. More than 90 % of pickings has a reading error less than or equal to 0.2 s. **(b)** Number of *P* and *S* phases identified for each station of STN and RSA networks. The dashed columns show the sum of the phases for stations SL03/SLA3 and SL05/SLA5, respectively, which correspond to different locations of the same station at nearby sites. **(c)** *P* and *S* readings error distribution for stations of STN and RSA networks. P5 and P95 indicate 5th and 95th percentile of the distribution and are represented by thin, grey bars; P25 and P75 indicate 25th and 75th percentiles and are represented by thick, coloured bars; P50 is the median and it is represented by the white thin line inside the thick bar. **(d)** *P* and *S* weight code histograms for all the 60 RSNC stations used in this study. Red and blue colour scales represent weight codes associated to *P* and *S* readings respectively.

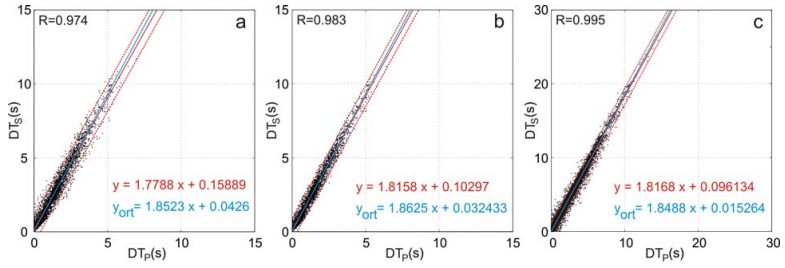

Fig. 6. Modified Wadati plot (Chatelain, 1978) of the arrival time dataset of this study. **(a)** Initial dataset of STN stations only. Red and blue lines represent ordinary least squares (with its standard deviation) and orthogonal regression, respectively. Coefficients are given in the formula. **(b)** As a, but after reading refinement and outlier removal. **(c)** Final diagram obtained after integration of other station's phase readings (either re-picked or as given by bulletins). Note the increase of linear correlation coefficient *R* from **(a)** to **(c)**, as well as the changes of V_P/V_S for the two different regressions. The ratio V_P/V_S 1.85 is the final value chosen.

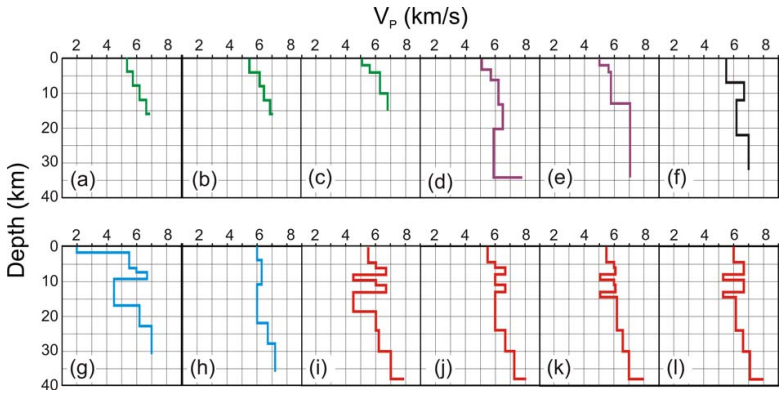

Fig. 7. Compilation of *P* wave velocity (V_P) models from literature for the Sulmona area. Models derive: **(a–e)** from seismological data; **(f–h)** from geophysical investigations; and **(i–l)** from geological interpretation. Key references are: **(a)** Bagh et al. (2007); **(b)** Chiarabba et al. (2009); **(c)** Chiarabba et al. (2010); **(d)** Chiarabba et al. (2005); **(e)** Chiarabba et al. (2005) modified; **(f)** Scarascia et al. (1994); **(g)** Patacca et al. (2008); **(h)** Di Luzio et al. (2009); **(i–l)** geostructural layering from Lavecchia and de Nardis (2009) and V_P from many sources (Patacca et al., 2008; Di Luzio et al., 2009; Barchi et al., 2003; Trippetta et al., 2013).

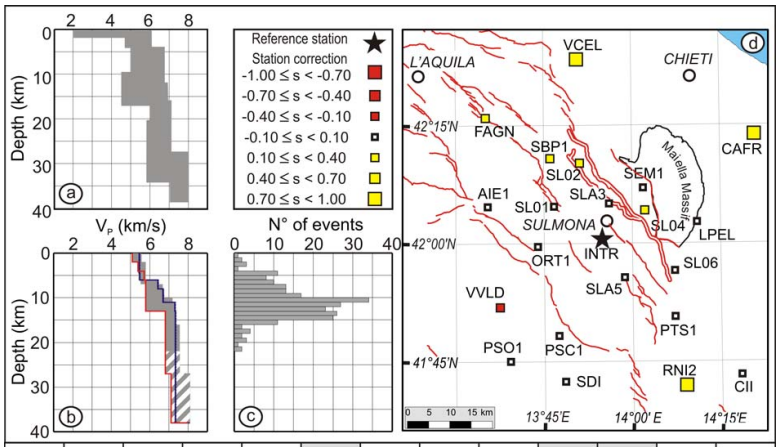

MODEL	(a)	(b)	(c)	(d)	(e)	(f)	(g)	(h)	(i)	(j)	(k)	(l)
first it.	0.387	0.442	0.419	0.404	0.435	0.429	0.590	0.496	0.539	0.491	0.440	0.576
last it.	0.111	0.111	0.114	0.113	0.110	0.114	0.121	0.117	0.110	0.110	0.112	0.119

Fig. 8. 1-D velocity model in the Sulmona area. **(a)** Envelope (e.g. range of variability) of the starting *P* wave velocity models individually plotted in Fig. 7. **(b)** Envelope (e.g. range of variability) of the best 1-D velocity models computed with the Velest code having a misfit less than or equal to 0.1 s. The stripped area represents the unconstraint depth interval of the velocity models. **(c)** Depth distribution of the selected events (Fig. 2) used to compute the velocity model. **(d)** Location map of the seismic network with station corrections related to the best model; positive values correspond to velocity slower with respect to the model. In the table are synthesized the start and final travel-time residual for each of the 12 used models (a–l in Fig. 7).

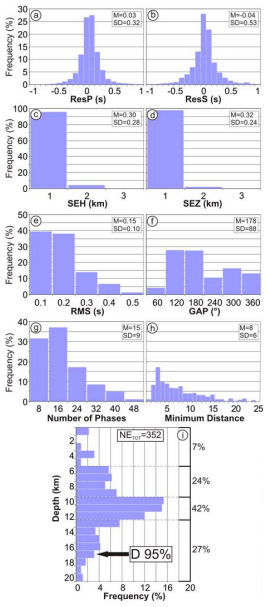

Fig. 9. Features of quality A earthquake locations. **(a, b)** Histograms of residuals of *P* and *S* phases (ResP, ResS). **(c, d)** Horizontal and vertical formal errors (SEH, SEZ). **(e, f)** Root mean square of travel time residuals (RMS) and GAP distribution. **(g, h)** Number of used phases and minimum hypocenter to station distance. From **(a)** to **(h)**, on the upper-right corners mean (M) and standard deviation (SD) of distributions are reported. **(i)** Depth distribution of the hypocenters. The black arrow identifies the seismogenic layer corresponding to the 95 % of the hypocentral distribution. On the right side are reported the percentages of the events occurred in the depth intervals 0–5 km, 5–9 km, 9–12 km, 12–17 km and deeper. Also the total number (NE_{TOT}) of quality A events is indicated.

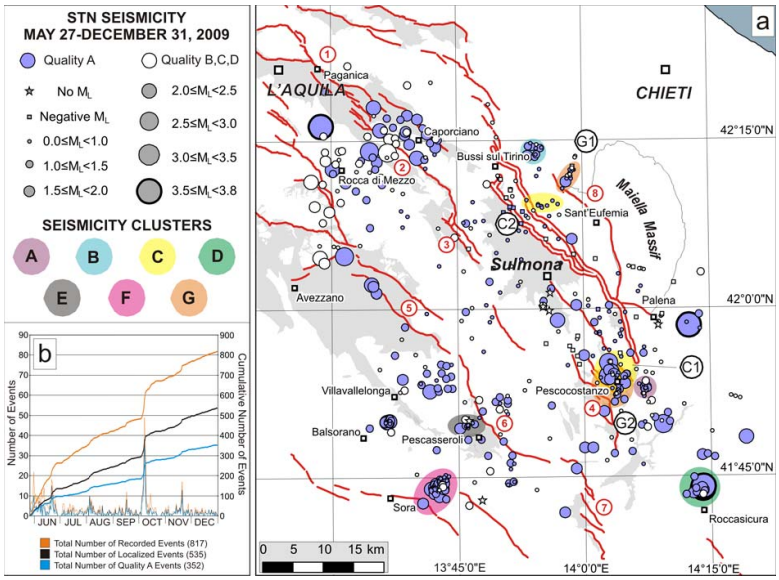

Fig. 10. Seismicity recorded by STN in the Sulmona area (Abruzzo region) from 27 May to 31 December 2009. **(a)** Epicentral distribution of the 535 events localized by using Hypoellipse (Lahr, 1980, 1984, 1999) and the best 1-D velocity model estimated for this area. Symbol colours refer to the quality of earthquake locations; symbol shape and dimension refer to their local magnitude. Coloured areas (A–G) point out the seismicity clusters corresponding to seismic swarms as described in the text. For location map of the represented area and legend see Fig. 1. **(b)** Number and cumulative number of earthquakes versus time; location quality is given with respect to relocated events, described in Sect. 5.

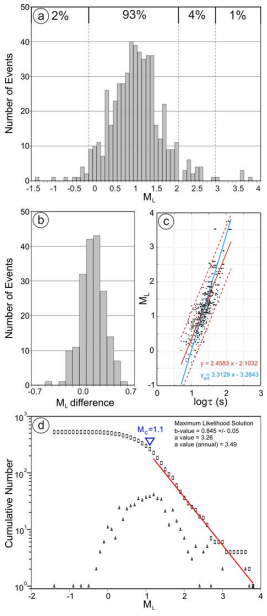

Fig. 11. (a) Histogram of M_L estimates of earthquakes localized in this study. On the top of the histogram are reported the percentages of the events within the corresponding range of magnitude. **(b)** Histogram of the residuals between local magnitude estimated in this study and that reported on ISIDE database, for coincident events. **(c)** Calibration of M_D magnitude, through linear regression of M_L against event duration (τ). In red and blue ordinary least squares and orthogonal regressions, respectively. Dashed lines represent the standard deviation of ordinary least squares regression. **(d)** Gutenberg–Richter slope evaluated with 527 events for which M_L has been estimated. In blue, the magnitude of completeness M_c.